phase, the following procedures were adopted: (i) the sample in this water-content region is heated at a scanning rate as low as 0.1 °C/min; (ii) the sample is annealed at temperatures just below the T_c and T_c* transition points for at least 6 h, respectively. On the basis of these procedures, any exothermic peak characteristic of transformation of the metastable phases into a more stable one was not observed in the heating direction and two endothermic peaks shown in run I of Figure 1b were not at all affected. This fact indicates that nuclear growth of the coagel phase requires a cooling procedure to crystallize the coexisting water, as is evident in run II of Figure 1b.

Finally, we want to discuss the present mode of phase transition in comparison with homologous systems of different counterions and different chain numbers previously investigated by us.

The octadecyltrimethylammonium bromide (OTAB) system,[2,12] which has a single chain, shows the same type of $G-T$ curves as those of the present system shown in Figure 5. On the other hand, the dioctadecyldimethylammonium chloride (DODAC),[3] which also has a double chain, exhibits a different type of the $G-T$ curves shown in Figure 7, similar to the octadecyltrimethylammonium chloride (OTAC) system.[1] The remarkable difference in two types of the $G-T$ curves shown in Figures 5 and 7 is the thermodynamic stability of the gel phase; the gel phase of chloride counterion exists in the stable state in the specified temperature region between the T_c and T_{gel} transitions, while the gel phase of bromide counterion exists in the metastable state over all temperatures below the T_c transition. However, the simultaneous appearance of the T_c and T_c* transitions observed in the intermediate-water-content region of the present system is not observed in the OTAB system,[2] although the mode of the $G-T$ curves is the same for both systems. Presumably, this may be concerned with a smaller T_c transition entropy (ΔS_c = 205 J/(K·mol)) of the OTAB system over all water contents and, consequently, a higher stability of the gel phase, compared with that of the gel phase of the DODAB system. Furthermore, when the T_c transition entropy of the DODAB system is compared with a total entropy change associated with the transformation from the coagel to liquid crystal phases of the DODAC system, these double-chain systems exhibit nearly the same value as shown in Figures 5 and 7. The corresponding entropy change is also nearly the same between the single-chain systems of OTAB and OTAC. However, the T_c transition entropy of the double-chain systems is only 1.4 times larger than that of the single-chain systems and is smaller than that expected. As is well-known, a drastic change at the T_c transition is attributed to a conformational change of the hydrocarbon chain. The small value of the T_c transition entropy of the double-chain systems indicates that the molecular motion of the hydrocarbon chain of these systems is fairly restricted, even at temperatures above the T_c transition, which is away from the generally accepted liquidlike state. This is connected with the formation of the liquid crystal phase of the double-chain systems above the T_c transition,[6-8] in contrast with that of the micellar solution phase of the single-chain systems.

Summarizing the above discussion of the homologous systems of different counterions and different chain numbers, it may be concluded that the halide counterion determines whether the gel phase exists in the thermodynamics stable or metastable states *at temperatures below the T_c transition*, which is intimately concerned with the mode of the phase transition. The number of hydrocarbon chains determines the aggregation state of amphiphile molecules, micelle and/or liquid crystal, *at temperatures above the T_c transition.*

Coadsorption of Carbon Monoxide and Hydrogen on the Ni(100) Surface: A Theoretical Investigation of Site Preferences and Surface Bonding

Jing Li, Birgit Schiøtt,† Roald Hoffmann,* and Davide M. Proserpio‡

Department of Chemistry and Materials Science Center, Cornell University, Ithaca, New York 14853-1301
(Received: May 16, 1989; In Final Form: August 18, 1989)

The CO/H coadsorption on the Ni(100) surface is discussed in this study. Relative stabilities of various possible surface structures are compared for the initial state (lower temperature form), as well as the final state (higher temperature form) of the coadsorption system. The surface–adsorbate bonding in the Ni(100)/H(4)/CO(t) structure (H(4) stands for hydrogen atoms adsorbed in a 4-fold hollow site and CO(t) stands for carbon monoxide in the on-top position), the most favorable choice of the lower temperature state, resembles that of the singly adsorbed systems. The adsorbate–adsorbate interaction does not lead to any chemical bonds but does affect the surface–CO π bonding. Destabilization of the CO 2π orbitals due to the 2π–1s(H) interaction results in a depopulation of the 2π states and a strengthening of the C–O bond. For the observed higher temperature c($2\sqrt{2}\times\sqrt{2}$)R45° geometry of CO, possible H and H_2 (adsorbed hydrogen molecule) arrangements in the final surface state are compared. Energy and crystal overlap population analyses show that the 4-fold adsorption site for both H and H_2 gives good agreement with the experimental observations. A new adsorbate–adsorbate coupling between CO(t) and H_2(4) (hydrogen molecule adsorbed in a 4-fold hollow site) is seen, but this coupling does not significantly affect the surface–adsorbate bonding. Again, no C–H or O–H bonds are formed. Besides the favorable CO(t)/CO(4) (half of the CO's adsorbed terminally and the other half in the 4-fold hollow site) configuration, our calculations also reveal the possibility of a CO(t)/CO(b) combination (half of the CO's adsorbed terminally and the other half in a bridging manner) in the final state.

There have been many studies of the coadsorption of carbon monoxide and hydrogen on the various transition-metal surfaces during the past 10 years. Examples among these include many close-packed faces such as Ni(111),[1-3] Pt(111),[4] Rh(111),[5] Pd(111),[6,7] and Ru(001)[8] and more open faces such as W(100),[9-12] Rh(100),[13,14] Fe(100),[15] and Ni(100).[16-27] The great activity in

† Department of Chemistry, University of Aarhus, DK-8000 Aarhus C, Denmark.
‡ Istituto di Stereochimica ed Energetica dei Composti di Coordinazione, C. N. R., via J. Nardi 39, 50132-Florence, Italy.

(1) Conrad, H.; Ertl, G.; Küppers, J.; Latla, E. E. *Proc. Int. Congr. Catal., 6th* **1977**, 427.
(2) Bertolini, J. C.; Imelik, B. *Surf. Sci.* **1979**, *80*, 586.
(3) Peebles, D. E.; Creighton, J. R.; Belton, D. N.; White, J. M. *J. Catal.* **1983**, *80*, 482.
(4) Baldwin, Jr., V. H.; Hudson, J. B. *J. Vac. Sci. Technol.* **1971**, *8*, 49.

0022-3654/90/2094-1554$02.50/0

this area arises mainly because of the importance of these systems to the understanding of many surface chemical reactions, for example, the Fischer–Tropsch and methanation processes.

Numerous experiments have shown that segregation of CO/H adsorbates is a common feature on the close-packed surfaces, whereas on the more open surfaces, e.g., fcc(100) and bcc(100), strong interactions between the coadsorbed species are detected. Particular attention has been drawn to the Ni(100)/H/CO system, which exhibits a new low-temperature desorption state, the so-called Σ-desorption, around 210 K for both CO and H_2 in temperature-programmed desorption (TPD).[17,18,21,22,24,25] This is an indication of the presence of strongly coupled CO- and H-derived surface species.[22]

How do the adsorbed carbon monoxide, CO(a), and the adsorbed hydrogen atoms, H(a), interact on the Ni(100) surface? What are the favorable sites for the coadsorption at a certain temperature? These questions have been subjects of both experimental and theoretical investigations and form the main subject of this study.

In two very recent papers,[26] Andersson et al. proposed that the coadsorption process gives rise to an initial structure, Ni(100)-p(1×1)H-c(2×2)CO at 80 K. This state transforms irreversibly into a $(2\sqrt{2}\times\sqrt{2})R45°$ structure at a higher temperature of ~150 K. During the transformation process, some of the adsorbed CO molecules change adsorption sites from the on-top position to the 4-fold hollow site and some of the adsorbed hydrogen atoms recombine to form chemisorbed H_2 molecules. A detailed discussion of such a transformation, including possible sites for the coadsorbed CO, H, and H_2, is given in the last part of this study. In the first part of the analysis we will focus on the initial adsorption state, on the electronic structures of the different surface configurations, and on the interactions between the adsorbates and the metal surface as well as between the coadsorbed species. Comparisons are made between the single adsorbate systems and the coadsorbate system, in order to gain a better understanding of how CO and H behave in the coadsorption process. The extended Hückel[28] tight-binding[29] approach is used throughout the paper, and the relevant atomic parameters are listed in the Appendix.

CHART I

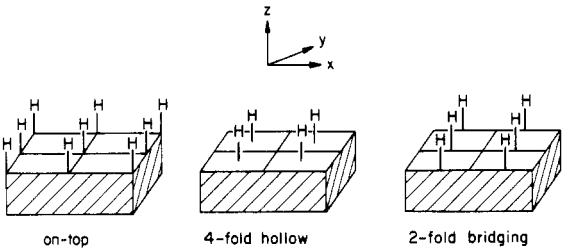

TABLE I: Electron Densities and Overlap Populations for the Ni(100) Clean Surface and the Ni(100)/H(4) Surface

	Ni(100) + H[a]	Ni(100)/H(4) surface
	Electron Density[b]	
$3d_{x^2-y^2}$	1.716	1.735
$3d_{z^2}$	1.923	1.901
$3d_{xy}$	1.901	1.579
$3d_{xz,yz}$	1.897	1.841
$4s + 4p_z$	0.628	0.516
1s(H)	1.000	1.424
	Overlap Population	
Ni(s)–Ni(s)	0.150	0.089
Ni(s)–H(4)		0.146
Ni(b)–H(4)[c]		0.021

[a] Separated Ni(100) clean surface and a H atom. [b] Only the electron densities of the surface Ni [Ni(s)] atomic orbitals are listed. [c] Ni(b) = nickel bulk atom; H(4) = H atom in the 4-fold hollow site.

H_2 Adsorption on the Ni(100) Clean Surface

First we consider the adsorption of H_2 on the Ni(100) clean surface, a most extensively studied chemisorption system. The process has been found to be dissociative, from adsorption–desorption kinetics[30-32] and from the EELS experiments of the hydrogen–deuterium exchange reaction.[33] From the vibrational properties of the hydrogen atoms adsorbed on the Ni(100) surface, it is suggested that they adsorb in the 4-fold hollow site.[33-35] With low-energy electron diffraction (LEED), different ordered surface structures at different temperatures have been observed. At 100 K, a well-ordered p(1×1)H surface layer is formed, giving rise to a saturation coverage of $\theta_H = 1.0$.[32,36,37] At 200 K, a quasi-ordered p(2×2)H layer is formed with $\theta_H = 0.25$.[33] A number of theoretical calculations have compared the binding energies of the hydrogen-adsorbed Ni(100) surfaces with H atoms at three different high-symmetry sites. In an early report by Fassert et al.,[38] it was suggested that the on-top site is slightly more favorable than the 4-fold hollow site and the 2-fold bridging site. More recent studies[39,40] show that the 4-fold hollow site represents the energetically most stable site for hydrogen adsorption, consistent with the experimental observations. It should be pointed out that the binding energies obtained from various theoretical studies all

(5) Williams, E. D.; Thiel, P. E.; Weinberg, W. H.; Yates, Jr., J. T. *J. Chem. Phys.* **1980**, *72*, 3496.
(6) Kiskinova, M. P.; Bliznakov, G. M. *Surf. Sci.* **1982**, *123*, 61.
(7) Kok, G. A.; Noordermeer, A.; Nieuwenhuys, B. E. *Surf. Sci.* **1983**, *135*, 65.
(8) Peebles, D. E.; Schreifels, J. A.; White, J. M. *Surf. Sci.* **1982**, *116*, 117.
(9) Yates, J. T.; Madey, T. E. *J. Chem. Phys.* **1971**, *54*, 4969.
(10) Vorburger, T. V.; Sandstrom, D. R.; Waclawski, B. J. *Surf. Sci.* **1976**, *60*, 211.
(11) Benziger, J.; Madix, R. J. *Sur. Sci.* **1978**, *77*, 657.
(12) Benziger, J.; Madix, R. J. *J. Vac. Sci. Technol.* **1978**, *15*, L379.
(13) (a) Kim, Y.; Peebles, H. C.; White, J. M. *Surf. Sci.* **1982**, *114*, 363. (b) Peebles, D. E.; Peebles, H. C.; White, J. M. *Surf. Sci.* **1984**, *136*, 463.
(14) (a) Richter, L. J.; Gurney, B. A.; Ho, W. *J. Chem. Phys.* **1987**, *86*, 477. (b) Richter, L. J.; Germer, T. A.; Ho, W. *Surf. Sci.* **1988**, *195*, L182.
(15) Benziger, J. B.; Madix, R. J. *Surf. Sci.* **1982**, *115*, 279.
(16) Andersson, S. *Proc. Int. Vac. Congr. 7th* **1977**, 1019.
(17) Yates, Jr., J. T.; Goodman, D. W.; Madey, T. E. *Proc. Int. Vac. Congr. 7th* **1977**, 1133.
(18) Goodman, D. W.; Yates, Jr., J. T.; Madey, T. E. *Surf. Sci.* **1980**, *93*, L135.
(19) Koel, B. E.; Peebles, D. E.; White, J. M. *Surf. Sci.* **1981**, *107*, L367.
(20) Koel, B. E.; Peebles, D. E.; White, J. M. *J. Vac. Sci. Technol.* **1982**, *20*, 889.
(21) Peebles, H. C.; Peebles, D. E.; White, J. M. *Surf. Sci.* **1983**, *125*, L87.
(22) Koel, B. E.; Peebles, D. E.; White, J. M. *Surf. Sci.* **1983**, *125*, 709, 739.
(23) White, J. M. *J. Phys. Chem.* **1983**, *87*, 915.
(24) Mitchell, G. E.; Gland, J. L.; White, J. M. *Surf. Sci.* **1983**, *131*, 167.
(25) Peebles, D. E.; Peebles, H. C.; Belton, D. N.; White, J. M. *Surf. Sci.* **1983**, *134*, 46.
(26) Westerlund, L.; Jönsson, L.; Andersson, S. *Surf. Sci.* **1987**, *187*, L669; **1988**, *199*, 109.
(27) Gland, J. L.; Shen, S.; Zaera, F.; Fischer, D. A. *J. Vac. Sci. Technol.* **1988**, *A6*, 2426.
(28) (a) Hoffmann, R. *J. Chem. Phys.* **1963**, *39*, 1397. (b) Hoffmann, R.; Lipscomb, W. N. *J. Chem. Phys.* **1962**, *37*, 2872. (c) Ammeter, J. H.; Burgi, H.-B.; Thibeault, J. C.; Hoffmann, R. *J. Am. Chem. Soc.* **1978**, *100*, 3686.
(29) (a) Whangbo, M.-H.; Hoffmann, R. *J. Am. Chem. Soc.* **1978**, *100*, 6093. (b) Hoffmann, R. *Solids and Surfaces: A Chemist's View of Bonding in Extended Structures*; VCH Publishers: New York, 1988. (c) Hoffmann, R. *Rev. Mod. Phys.* **1988**, *60*, 601.
(30) Lapujoulacle, J.; Neil, K. S. *Surf. Sci.* **1973**, *35*, 288.
(31) Christmann, K.; Schober, O.; Ertl, G.; Neumann, M. *J. Chem. Phys.* **1974**, *60*, 4528.
(32) Christmann, K. *Z. Naturforsch.* **1979**, *34A*, 22.
(33) Andersson, S. *Chem. Phys. Lett.* **1979**, *42*, 472.
(34) Upton, T. H.; Goddard, W. A. *Phys. Rev. Lett.* **1979**, *42*, 472.
(35) Nordlander, P.; Holloway, S.; Nørskov, J. K. *Surf. Sci.* **1983**, *136*, 59.
(36) Rieder, K. H.; Wilsch, H. *Surf. Sci.* **1983**, *131*, 245.
(37) Karlsson, P.-A.; MÅrtensson, A.-S.; Andersson, S. *Surf. Sci.* **1986**, *175*, L759.
(38) Fassert, D. J. M.; van der Avoird, A. *Surf. Sci.* **1976**, *55*, 291.
(39) Nørskov, J. K. *Phys. Rev. Lett.* **1982**, *48*, 1620.
(40) Umrigar, C.; Wilkins, J. W. *Phys. Rev. Lett.* **1985**, *54*, 1551.

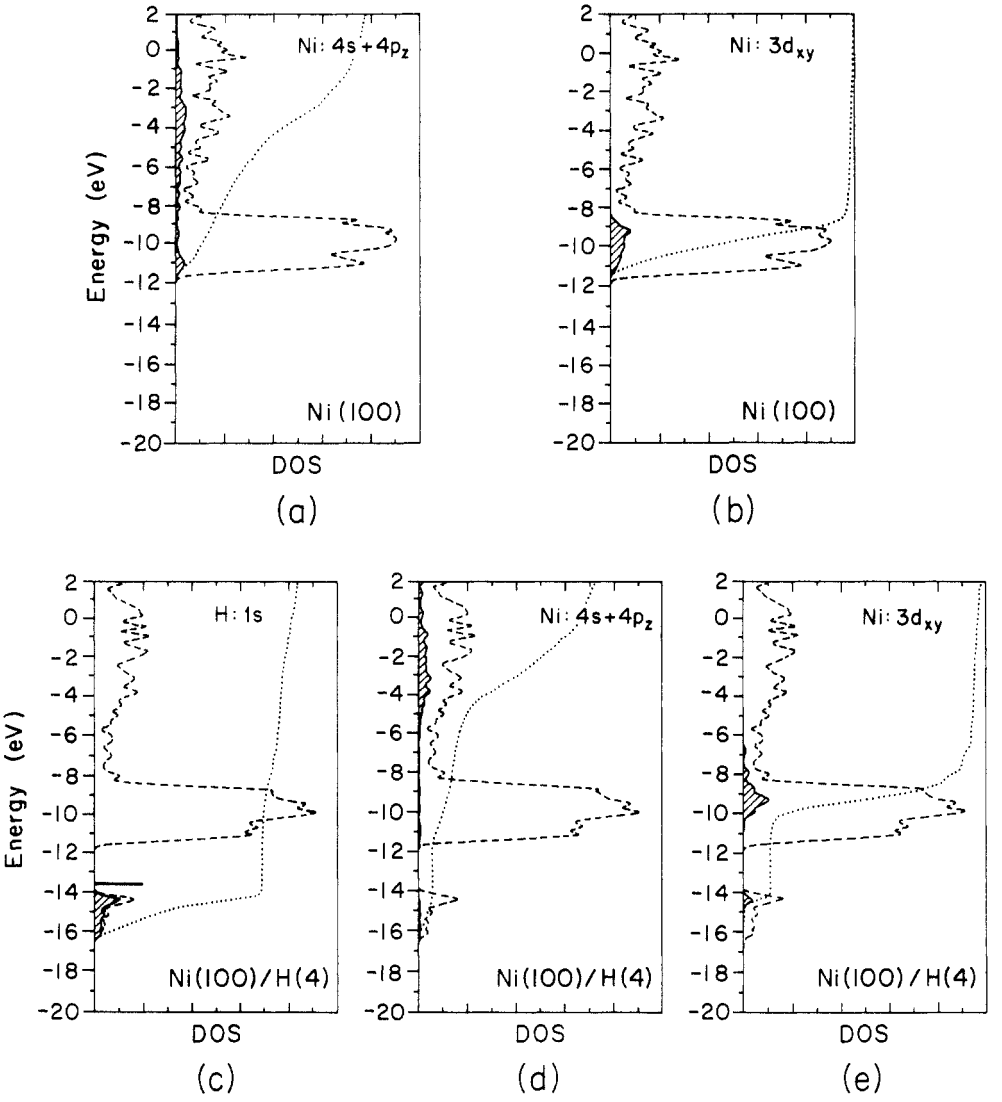

Figure 1. Some projected density of states (shaded area) for the Ni(100) clean surface and the Ni(100)/H(4) surface: (a) contribution of the surface Ni 4s + $4p_z$ on the Ni(100) surface; (b) the $3d_{xy}$ states of a surface Ni on the same surface; (c) H 1s contribution to the total DOS in the Ni(100)/H(4) system; (d) Ni(s) 4s + $4p_z$ density of state projection in the same system; and (e) Ni(s) $3d_{xy}$ contribution. Dotted lines give integrations of the projected states, and dashed lines are the total DOS. The horizontal stick in (c) indicates orbital energy of an atomic hydrogen 1s.

give very small differences for the three adsorption sites. As a comparison, we have also computed the binding energies for the three surface structures shown in Chart I. We define the binding energy in such a way that the higher the positive value, the more stable the system under the consideration. The results are indeed very similar for the three cases: the on-top adsorption has a binding energy of 0.06 eV higher than that of the 4-fold hollow structure and of 0.18 eV higher than that of the 2-fold bridging structure.

Determination of the bond distance of the adsorbed hydrogen at the 4-fold hollow site to the surface Ni atoms has turned out to be rather difficult experimentally. Two values have been reported so far, 0.9–1.0 Å (the height of the hydrogen atoms above the first Ni layer) from He diffraction measurement[36] and 0.5 ± 0.1 Å (corresponding to a Ni–H distance of 1.83 Å) from the transmission channeling experiments under ultrahigh-vacuum conditions.[41] On the theoretical side things are not much clearer. A Hartree–Fock calculation on a Ni cluster[34] and the linear augmented plane-wave method applied to a Ni slab[42] give the same value of 0.3 Å; a larger value, 0.8 Å, is produced with the effective medium theory.[39] Using the extended Hückel tight-binding approach, we have obtained an energy minimum at a Ni(s)–H(4) distance (where Ni(s) stands for a surface Ni atom) of ~1.78–1.80 Å, in good agreement with the result from the transmission channeling experiment, and of 1.79 Å from the density functional total energy calculations.[40] A value of 1.8 Å is thus chosen for the Ni(s)–H(a) bond distance in the analysis hereafter. It should be kept in mind, however, that good bond distance predictions are not typical of extended Hückel calculations.

Listed in Table I are the electron densities and the overlap populations[29b] for both the Ni(100) clean surface and the Ni(100)/H system with H adsorbed in the 4-fold hollow site, the experimentally suggested surface structure. The most significant change in the electron density of a surface Ni atom upon hydrogen adsorption clearly comes from its $3d_{xy}$ orbital which "points" toward the hollow sites above which the hydrogen sits: a loss of 0.3 electron is computed. Another 0.1 electron loss is from the Ni(s) 4s + $4p_z$ orbitals. The total loss of 0.4 electron from a Ni(s) atom is gained by the adsorbed hydrogen atom at the 4-fold hollow site, H(4). The direction of electron transfer is thus from surface Ni to the hydrogen atoms. In general, electron-withdrawing species cause an increase in the work function of the surface and a decrease in the occupied density of states of the d bands.[43] This is indeed the situation. The work function increase for the Ni(100)/H system has been reported to be $\Delta\phi = +0.17$ eV.[31] Our calculated d-band occupation of a Ni(s) atom shows a decrease of 0.44 electron up to the Fermi level. One should be aware,

(41) Stensgaard, I.; Jacobsen, F. *Phys. Rev. Lett.* **1985**, *54*, 711.
(42) Umrigar, C.; Wilkins, J. W. *Bull. Am. Phys. Soc.* **1984**, *29*, 434.
(43) Nieuwenhuys, B. E. *Surf. Sci.* **1981**, *105*, 505.

CHART II

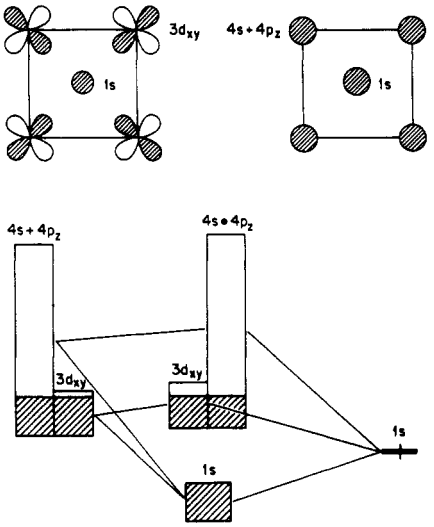

however, that the extended Hückel calculations tend to exaggerate electron flows.

Some projected density of states (DOS) curves are depicted in Figure 1. Plotted in Figure 1, a and b, are the DOS of the Ni(s) 4s + 4p$_z$ and 3d$_{xy}$ orbitals of the clean surface, respectively; and in Figure 1, d and e, are the corresponding orbitals of the 4-fold adsorbed hydrogen surface. Figure 1c gives the hydrogen 1s orbital contribution to the total DOS.

A simple diagram shown in Chart II describes schematically how an H(4) atom interacts with the surface Ni atoms. Its greater part is pushed down, significantly so compared to its atomic energy (indicated by a horizontal stick in Figure 1c). Most of the Ni(s) 3d$_{xy}$ states are lifted up, and about 6% of the Ni(s) 4s + 4p$_z$ orbitals appear in the −14 to −16 eV region, indicating their participation in bonding with the H(4) atoms. Other metal orbitals (not shown in the figure) remain almost unchanged. Returning to Table I, we see that strong Ni(s)–H(4) bonds (an overlap population of 0.146) are formed during the adsorption process, although compensated by weakening of some surface–surface and surface–bulk Ni–Ni bonds.

CO Adsorption on the Ni(100) Clean Surface

Chemisorption of CO on the Ni(100) surface is certainly another popularly investigated system. Experimentally, it has been confirmed that CO adsorbs molecularly and takes on an upright orientation, with the carbon atom bonded to the Ni surface.[44-46] The adsorption sites of CO depend strongly on the temperature and the coverage.[47] An exposure of ~2 langmuirs (1 langmuir = 10^{-6} Torr·s) at 295 K results in a c(2×2)CO surface structure with a CO on-top adsorption geometry and a coverage of θ_{CO} = 0.5.[16]

An analysis of the chemisorption of CO on various transition-metal surfaces, concentrating on the Ni(100) surface, have been made earlier by our group.[48] There has also been many other theoretical studies, references to which may be found in that paper (ref 48). There, a four-layer slab model was employed with CO adsorbed on one side of the slab. The Ni–C distance was taken as 1.8 Å and the C–O distance as 1.15 Å.[46] In the present study, we have used the same distances but have chosen a three-layer slab instead of a four-layer slab. In fact, nearly identical results are obtained.

As expected, the CO 5σ orbital interacts strongly with the Ni 3d$_{z^2}$ and its 4s + 4p$_z$ states. Electron densities and important crystal orbital overlap populations (COOP)[29b,49] are compared in Table II for the Ni(100) clean surface and the Ni(100)/CO(t) surface, where CO(t) is a label for the carbon monoxide adsorbed at an on-top position. A loss of ~0.4 electron from the 5σ orbital is computed due to the strong 3d$_{z^2}$–5σ interaction. Much of the 3d$_{z^2}$ state, mostly 3d$_{z^2}$–5σ antibonding, is pushed above the Fermi level, enhancing the metal–CO σ bonding.[48] The back-donation from metal d$_\pi$ orbitals (3d$_{xz}$ and 3d$_{yz}$) results in a gain of 0.75 electron to the CO 2π orbitals. An overlap population of 0.845 is obtained between the Ni(s,CO) (surface Ni atom that is directly bonded to CO) and the carbon atom, indicating a strong surface–adsorbate bonding. The interested reader is referred to the previous report (ref 48) for a more complete analysis.

TABLE II: Electron Densities and Overlap Populations for the Ni(100) Clean Surface and the Ni(100)/CO(t) Surface

	Ni(100) + CO[a]	Ni(100)/CO(t) surface
Electron Density		
Ni(s,CO)[b]		
3d$_{x^2-y^2}$		1.702
3d$_{z^2}$		1.451
3d$_{xy}$		1.954
3d$_{xz,yz}$		1.658
Ni(s)		
3d$_{x^2-y^2}$	1.716	1.630
3d$_{z^2}$	1.923	1.923
3d$_{xy}$	1.901	1.937
3d$_{xz,yz}$	1.897	1.887
CO(t)[b]		
4σ	2.000	1.884
1π	4.000	4.000
5σ	2.000	1.621
2π	0.000	0.748
Overlap Population		
Ni(s,CO)–C		0.845
C–O	1.207	1.043

[a] Separated Ni(100) clean surface and a CO molecule. [b] Ni(s,CO) = Ni atom that directly bonds to CO; CO(t) = terminally adsorbed CO.

CO/H Coadsorption on Ni(100): The Lower Temperature State

We now turn to the coadsorption process. As mentioned previously, an initial state of the Ni(100)/H/CO surface is formed at 80 K. From the vibrational frequencies measured by the EELS experiments, it was suggested[26] that the coadsorbed hydrogen atoms, as in the single adsorbate Ni(100)-p(1×1)H system,[37] occupy the 4-fold hollow site, giving rise to a coverage of θ_H = 1.0 (**1**). Likewise, the coadsorbed CO molecules take the on-top position, as in the single adsorbate case, producing a lattice structure of Ni(100)-c(2×2)CO with a CO coverage of θ_{CO} = 0.5 (**2**).

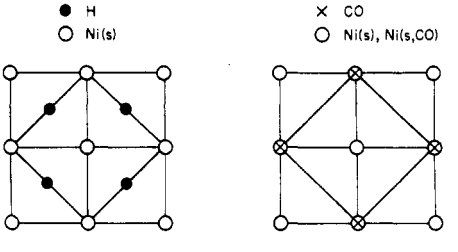

1 **2**

To see whether our results support the experimentally proposed adsorption sites for H and CO, we have performed a set of calculations on seven Ni(100)-p(1×1)H-c(2×2)CO surface structures, all with θ_{CO} = 0.5 and θ_H = 1.0. It should be pointed out here the computational limitations prevent us from discussing the possibility of island formation and/or CO/H segregation which

(44) Allyn, C.; Gustafsson, T.; Plummer, E. *Solid State Commun.* **1978**, *28*, 85.
(45) Passler, M.; Ignatiev, A.; Jona, F.; Jepsen, D.; Marcus, P. *Phys. Rev. Lett.* **1979**, *43*, 360.
(46) Andersson, S.; Pendry, J. *Phys. Rev. Lett.* **1979**, *43*, 363.
(47) Andersson, S. *Solid State Commun.* **1977**, *21*, 75.
(48) Sung, S.-S.; Hoffmann, R. *J. Am. Chem. Soc.* **1985**, *107*, 578.
(49) Hughbanks, T.; Hoffmann, R. *J. Am. Chem. Soc.* **1983**, *105*, 1150.

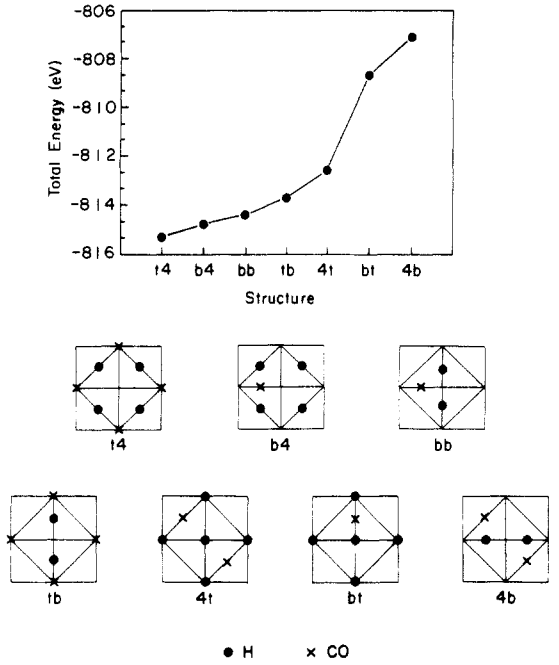

Figure 2. Calculated total energies for the seven Ni(100)-p(1×1)H-c(2×2)CO surface structures. A two-dimensional view of each configuration is given at the bottom of the plot.

CHART III

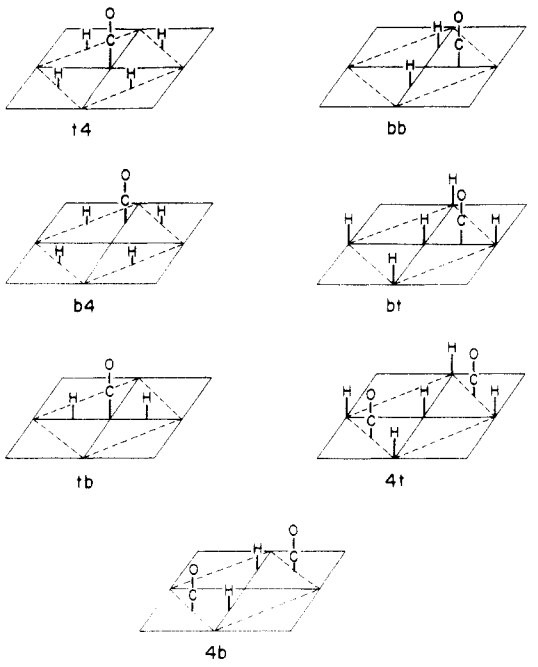

may occur during the coadsorption process. This would require very large unit cells. These structures are sketched in Chart III, where the labels under each structure specify the adsorption sites of CO and H, respectively. **t** stands for an on-top site, **4** means a 4-fold hollow site, and **b** means a 2-fold bridging site. The CO site is given first and then the H one.

The relative total energies obtained for all seven configurations are plotted in Figure 2. Obviously, the **t4** structure represents energetically the most stable surface structure, whereas the **4b** (CO in the 4-fold hollow site and H in the 2-fold bridging site) and **bt** (CO in the 2-fold bridging site and H in the on-top site) are the least stable structural choices. The strength of the surface–adsorbate bonding is reflected in Figure 3, where the average overlap populations between the surface Ni atom and the adsorbates are shown for the seven structures. The **t4** configuration gives the strongest Ni–CO bond, with a Ni(s,CO)–C overlap population of 0.781. The **tb** structure, on the other hand, also

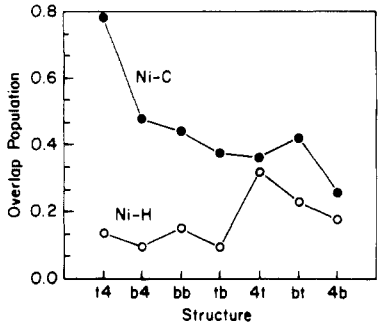

Figure 3. Crystal orbital overlap populations (COOP) of the Ni–C and Ni–H bonds for the seven Ni(100)-p(1×1)H-c(2×2)CO structures.

TABLE III: Electron Densities of the Ni(100) Clean Surface, Ni(100)/H(4) Surface, Ni(100)/CO(t) Surface, and the Ni(100)/H(4)/CO(t) Surface

	Ni(100)/H(4)	Ni(100)/CO(t)	Ni(100)/H(4)/CO(t)
Ni(s,CO)			
$3d_{x^2-y^2}$		1.702	1.827
$3d_{z^2}$		1.451	1.036
$3d_{xy}$		1.954	1.626
$3d_{xz,yz}$		1.658	1.649
Ni(s)			
$3d_{x^2-y^2}$	1.735	1.630	1.733
$3d_{z^2}$	1.901	1.923	1.892
$3d_{xy}$	1.579	1.937	1.636
$3d_{xz,yz}$	1.841	1.887	1.876
CO(t)			
4σ		1.884	1.878
1π		4.000	3.999
5σ		1.621	1.567
2π		0.748	0.607
H(4)			
1s	1.424		1.378

with CO sitting at the on-top position, has a much weaker Ni(s,CO)–CO bond; an overlap population of 0.377 is computed for this structure. The calculated metal–hydrogen overlap population values are similar for all structures in which H atoms occupy the 4-fold hollow site or the 2-fold bridging site. With the on-top site geometry as **4t** and **bt**, the bonding between surface Ni and H reaches its maximum, giving rise to an OP (overlap population) value of 0.318 and 0.228 for **4t** and **bt**, respectively. Although benefiting from the strong metal–hydrogen bonding, these two geometries are not likely to be good candidates for the stable coadsorption state, due to their high energies compared with, say, the **t4** geometry. The energy differences are 6.6 and 2.7 eV, respectively. The instability of the **bt** structure is probably caused by the extremely short C–H distance (1.34 Å). That of **4t** is caused by the repulsive interaction between the adsorbed hydrogen and oxygen atoms through 1s(H) and 1π(CO) orbitals.[50]

We cannot trust the absolute energies computed from extended Hückel calculations completely. Nevertheless, it seems that the **t4** geometry (or the Ni(100)/H(4)/CO(t) structure), with the lowest average total energy and the strongest Ni(s,CO)–CO bonding, should be one of the best candidates for the initial state of the coadsorption process. To understand its electronic structure, let us first take a look at Table III, where the electron densities are listed for the Ni(100)/H(4) surface (single adsorbed H atoms in the 4-fold hollow site), the Ni(100)/CO(t) surface (single adsorbed CO at the on-top position), and the coadsorbed Ni(100)/H(4)/CO(t) surface. Compared with the Ni(100)/CO(t) surface, we notice that the most dramatic changes in the **t4** structure appear in the Ni(s,CO) $3d_{z^2}$ and the CO(t) 2π orbitals, where a loss of 0.42 and 0.14 electron is found. Decreases in

(50) The repulsive interaction of the hydrogen and oxygen is reflected in the overlap population between the two atoms. A negative value of −0.063 is obtained from our calculation.

CHART IV

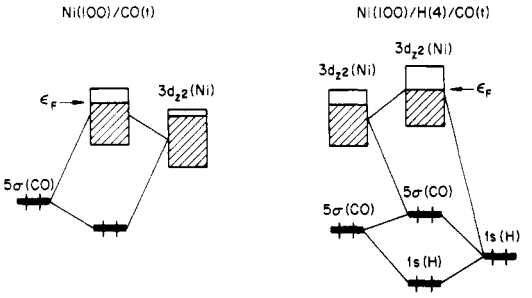

CHART V

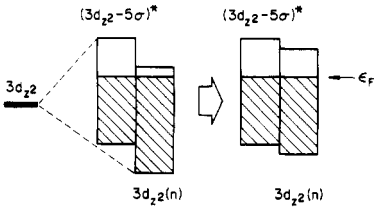

electron density of 0.33 and 0.30 electron for the Ni(s,CO) $3d_{xy}$ and Ni(s) (surface Ni atom that is not bonded to a CO) $3d_{xy}$ orbitals do not imply any interactions of a new type but are due to the mixing of these metal orbitals with the H(4) orbitals, which resembles what has been described in the Ni(100)/H(4) single adsorbate system. An depletion of 0.32 electron is calculated for the Ni(s) $3d_{xy}$ orbital there.

The changes in electron densities of the Ni(s,CO) $3d_{z^2}$ and the CO(t) 2π states are obviously caused by the coadsorbed species, that is, H(4) atoms. Chart IV depicts schematically what happens to the Ni(s,CO) $3d_{z^2}$ orbitals with and without H(4) involved in the adsorption process. The σ interaction between $3d_{z^2}$ of Ni(s,CO) and 5σ of CO(t) shown at left of Chart IV for the single adsorbate system has been discussed previously:[48] some of the $3d_{z^2}$ states, mainly $3d_{z^2}-5\sigma$ antibonding, are lifted up above the Fermi level (ϵ_F), resulting in a loss of 0.55 electron (see Table II). For the coadsorption process, as shown at the right of Chart IV, the hydrogen 1s orbital interacts strongly with CO(t) 5σ and pushes most of its states up (Figure 4). The $5\sigma-3d_{z^2}$ interaction is strengthened; about 20% of the $3d_{z^2}$ states contribute in the 5σ region compared with ~6% in the single adsorption case (see Figure 4). On the other hand, more of its filled states are pushed up above ϵ_F, giving rise to another 0.42 loss in its electron density. The top panels in Figure 4 show the 5σ and $3d_{z^2}$ states of the Ni(100)/CO(t) system; the bottom panels the same contributions, as well as the H state, of the coadsorbed **t4** system.

Two facts that we shall point out here are as follows: (i) although by symmetry it is allowed, we find that the Ni(s,CO) $3d_{z^2}$ and H(4) 1s interaction is very small, due to both large energy difference and small overlap between the two orbitals; (ii) with the mixing of Ni(s,CO) 4s + $4p_z$ orbitals into its $3d_{z^2}$ (through second-order perturbation), the lower portion of the $3d_{z^2}$ band is mainly $3d_{z^2}$(n) (where n stands for nonbonding), **3**, and the upper portion, mostly $3d_{z^2}-5\sigma$ antibonding states, **4**. Compared to the

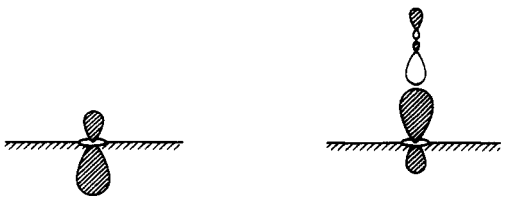

3 **4**

Ni(100)/CO(t) single adsorbed system, we see that it is the bottom part of the $3d_{z^2}$ band, that is, the $3d_{z^2}$(n) states, that are mostly pushed up above the Fermi level in the coadsorption process (Chart V). This can be confirmed from the $3d_{z^2}$ DOS projections shown in Figure 4. The $3d_{z^2}$(n)-5σ interaction may result in a slight increase in the Ni–CO σ bonding, but this increase is negligible (compared to the decrease in Ni–CO π bonding) due to the very small overlap between the two orbitals.

The central panel of Figure 4 shows the density of states contribution of H(4) atoms to the total DOS. One sees that about 8% of its states are distributed in the CO(t) 2π region (~−5 to −8 eV). The interaction between the CO(t) 2π and H(4) 1s orbitals is shown schematically in Chart VI; a fairly large part in the lower portion of the 2π band is lifted up, resulting in an electron loss of 0.14. The consequences of this are as follows: (i) strengthening of the C–O bond since the 2π orbitals are depopulated; an overlap population of 1.08 is calculated for this system compared with 1.04 obtained for the single adsorbed CO molecule; (ii) weakening of the metal–CO π bonding because of less interaction between the 2π and $3d_{xz}$ + $3d_{yz}$ orbitals. A decrease of 0.064 in overlap population is computed for the Ni(s,CO)–CO bond.

CHART VI

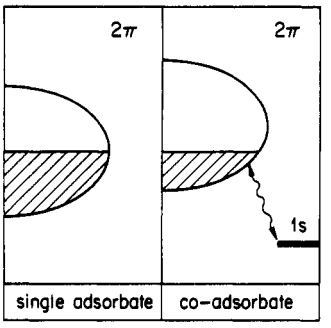

TABLE IV: EELS Data for the Single Adsorbed Systems Ni(100)/H(4) and Ni(100)/CO(t) and Coadsorbed System Ni(100)/H(4)/CO(t) and the Calculated Overlap Populations for the Corresponding Bonds

	Ni(100)/H(4)	Ni(100)/CO(t)	Ni(100)/H(4)/CO(t)
	Energy Loss, meV		
Ni–H	78		78
Ni–CO		60	50
C–O		256	258
	Overlap Population		
Ni–H	0.146		0.147
Ni–CO		0.845	0.781
C–O		1.042	1.080

Listed in Table IV are the Ni–H, C–O, and Ni–CO vibrational frequencies from the EELS experiments[26] for the three systems: Ni(100)/H(4), Ni(100)/CO(t), and Ni(100)/H(4)/CO(t). The calculated overlap populations for these bonds are also summarized in the table. Although not explicitly comparable to the measured frequencies, these give relative bond strengths. The values we obtain are indeed fully consistent with the experimental observations. Experimentally, the C–O stretching frequency is increased by 2 meV going from CO single adsorbed surface to CO/H coadsorbed surface, and we computed an increase of 0.04 in the C–O overlap population. The EELS data show that the most significant change occurs in the Ni–CO stretching frequency ($\Delta\nu$ = −10 meV), and that is also what we have obtained in our overlap population calculations. The measured Ni–H frequency remains unchanged for the single and coadsorbed systems, and a very small difference in its overlap population (0.001) is generated by our method. Comparisons of the overlap populations are also made for the other six surface configurations that we have studied. None of them give fully consistent agreement with the EELS data reported for Ni–H, Ni–CO, and C–O vibrational frequencies.

Thermal desorption studies, as well as ultraviolet photoemission spectroscopy (UPS) and high-resolution electron energy loss spectroscopy (HREELS) experiments,[19,21,22,25,26] have suggested that the dynamic coupling between adsorbed hydrogen and carbon

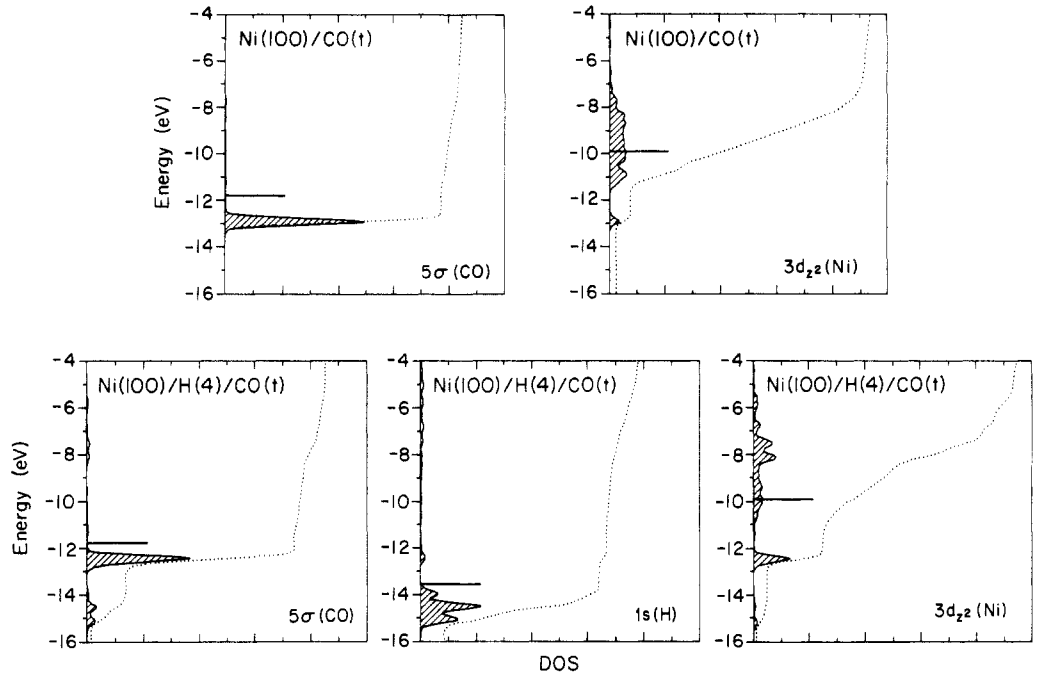

Figure 4. Density of state projections (shaded area) of some orbitals for the CO(t) single adsorbed surface, Ni(100)/CO(t), and for the H(4)/CO(t) coadsorbed surface, Ni(100)/H(4)/CO(t). The top panels plot out the DOS contributions from a CO(t) 5σ (left) and a Ni(s,CO) 3d_{z^2} (right) in the single adsorbed system, and the bottom panels, the corresponding orbitals in the coadsorbed system. The middle panel in the lower part of the figure gives the H 1s projection of the coadsorbed surface. The corresponding atomic and molecular orbital energies are indicated by horizontal sticks. Dotted lines give integration of the projected orbitals.

monoxide is strong, but neither C–H nor O–H bonds are formed on the coadsorbed surface. We have obtained a C–H overlap population of 0.02 for the **t4** system. Compared with that of a typical C–H bond, for example, 0.78 in a CH_4 molecule, this definitely cannot be considered as a chemical bond. However, the CO–H interaction does affect the metal–CO bonding, namely, the π interaction discussed above.

The work function measurements[21,25] on the Ni(100)–p(1×1)H–c(2×2)CO structure give a value of 0.3 eV above that of the Ni(100) clean surface. In accordance with these measurements, a total electron flow of 0.8 electron from the metal surface to the adsorbates is obtained for the Ni(100)/H(4)/CO(t) (**t4**) structure from our calculations.

CO/H Coadsorption on Ni(100): The Higher Temperature State

According to Westerlund and Andersson,[26] the initial low-temperature state of the CO/H coadsorbed system, Ni(100)–p-(1×1)H–c(2×2)CO, transforms to a stable (2$\sqrt{2}$×$\sqrt{2}$)R45° surface structure, **5**, at ~150 K. Although all three CO vibrational frequencies (on-top, 4-fold hollow, and 2-fold bridging) are observed in the EELS experiment, it is assumed[26] that the structure is built up primarily of CO molecules at the on-top and 4-fold positions since the energy loss peak at 235 meV (due to the bridging adsorbed CO) is very weak. In a later section we shall discuss the possibility of a surface structure with bridging adsorbed CO. The proposed structure thus has half of the CO molecules in the on-top positions, and the other half changing their positions, presumably into the 4-fold hollow sites which were initially occupied by the hydrogen atoms (**5b**). Since practically no desorption occurs during the structural transformation,[24] the CO and H coverages remain the same, $\theta_{CO} = 0.5$ and $\theta_H = 1.0$.[51] Part of the adsorbed H atoms recombine to form chemisorbed H_2 molecules, and the remaining atomic hydrogens stay in the 4-fold hollow sites. The coverage of the H(4) atoms is thus 0.5. There is, however, no direct information available about the geometrical arrangement of the chemisorbed H_2. Chemisorbed molecular H_2 is not a common species, which is in part responsible for the interest in these coadsorbed system. In discrete molecules several H_2 compounds have been recognized to date[52] following the discovery of the first one, $W(CO)_3(PR_3)_2(H_2)$.[53] The bonding in these has been studied by others.[54]

Taking into consideration the proposed CO and H adsorption sites, as well as their coverages, we have performed a set of calculations on six possible c(2$\sqrt{2}$×$\sqrt{2}$)R45° surface structures. These have H_2 in the 4-fold hollow sites, H_2(4); H_2 in the 2-fold bridging sites, H_2(b); and H_2 at the on-top positions, H_2(t). The Ni–C, Ni–H(4), and C–O distances are kept the same as in the preceding section, whereas the hydrogen–hydrogen bond in H_2 and the nickel–hydrogen bond between the surface metal and

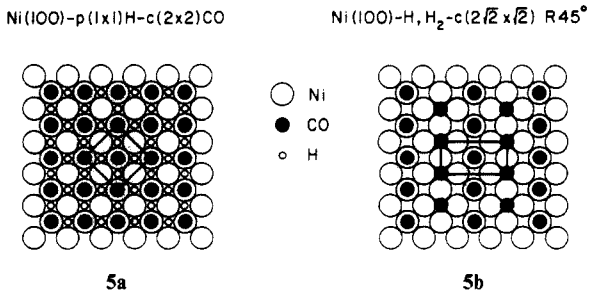

5a **5b**

(51) The coverage for the hydrogens here includes both adsorbed H atoms and H_2 molecules.

(52) See, for example: Morris, R. H.; Sawyer, J. F.; Shiralian, M.; Zubkowski, J. D. *J. Am. Chem. Soc.* **1985**, *107*, 5581. Church, S. P.; Gvevels, F.-W.; Herman, H.; Schaffner, K. *J. Chem. Soc., Chem. Commun.* **1985**, 30. Crabtree, R. H.; Lavin, M.; Bonneviot, L. *J. Am. Chem. Soc.* **1986**, *108*, 4032. Kubas, G. J.; Ryan, R. R.; Unkefer, C. J. *J. Am. Chem. Soc.* **1987**, *109*, 8113. Conroy-Lewis, F. M.; Simpson, S. J. *J. Chem. Soc., Chem. Commun.* **1987**, 1675. Bianchini, C.; Mealli, C.; Peruzzini, M.; Zanobini, F. *J. Am. Chem. Soc.* **1987**, *109*, 5548. Heinekey, D. M.; Payne, N. G.; Schulte, G. K. *J. Am. Chem. Soc.* **1988**, *110*, 2303. Hampton, C.; Cullen, W. R.; James, B. R. *J. Am. Chem. Soc.* **1988**, *110*, 6918. Costello, M. T.; Walton, R. A. *Inorg. Chem.* **1988**, *27*, 2563.

(53) Kubas, G. J.; Ryan, R. R.; Vergamini, P. J.; Wasserman, H. J. *J. Am. Chem. Soc.* **1984**, *106*, 451.

(54) Hay, P. J. *Chem. Phys. Lett.* **1984**, *103*, 466. Saillard, J.-Y.; Hoffmann, R. *J. Am. Chem. Soc.* **1984**, *106*, 2006. Lyons, D.; Wilkinson, G.; Thornton-Pett, M.; Hursthouse, M. B. *J. Chem. Soc., Dalton Trans.* **1984**, 695. Jean, Y.; Eisenstein, O.; Volatron, F.; Maouche, B.; Sefta, F. *J. Am. Chem. Soc.* **1986**, *108*, 6587. Hay, P. J. *J. Am. Chem. Soc.* **1987**, *109*, 705. Burdett, J. K.; Phillips, J. R.; Pourian, M. R.; Poliakoff, M.; Turner, J. J.; Upmacis, R. *Inorg. Chem.* **1987**, *26*, 3054. Burdett, J. K.; Pourian, M. R. *Inorg. Chem.* **1988**, *27*, 4445.

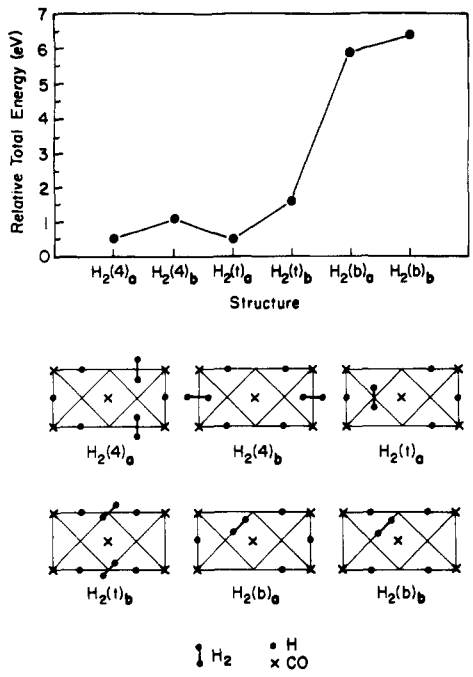

Figure 5. Plotted relative total energies for the six structures. A two-dimensional view of each structure is sketched in the lower portion of the figure.

CHART VII

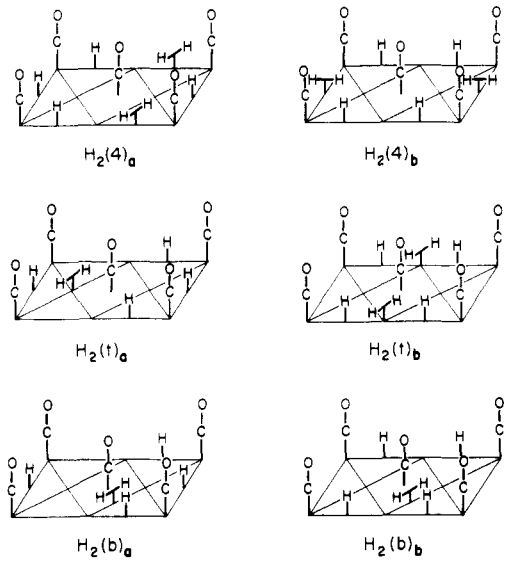

hydrogen in a H_2 molecule are taken to be 0.74 and 1.80 Å, respectively. These structural choices are indicated schematically in Chart VII. Notice that in all six cases half of the CO molecules take the on-top positions, $\theta_{CO(t)} = 0.25$, and the other half, the 4-fold hollow sites, $\theta_{CO(4)} = 0.25$. Atomic hydrogens are located in the rest of the 4-fold hollow sites with a coverage of $\theta_{H(4)} = 0.5$. Also notice that two geometrical arrangements (a and b) are described for each fixed H_2 location.

The average total energy (E_{tot}) curve for the six structures is plotted in Figure 5. The $H_2(b)$ geometries ($H_2(b)_a$ and $H_2(b)_b$ in Chart VII and Figure 5) give much higher values (~4–5 eV) than the others. These are apparently the least favorable choices for a stable surface structure. On the other hand, the structures with 4-fold and on-top adsorbed H_2 geometries, $H_2(4)$ and $H_2(t)$, are very close in their total energies. Thus, other criteria are necessary to make a decision about the structural preference.

Accompanying the structural transformation there is a work function increase of 0.2 eV.[21,25,26] Our calculated electron density changes to the adsorbates do give a positive value (i.e., electrons flow from surface to the adsorbed species) for both $H_2(4)$ and

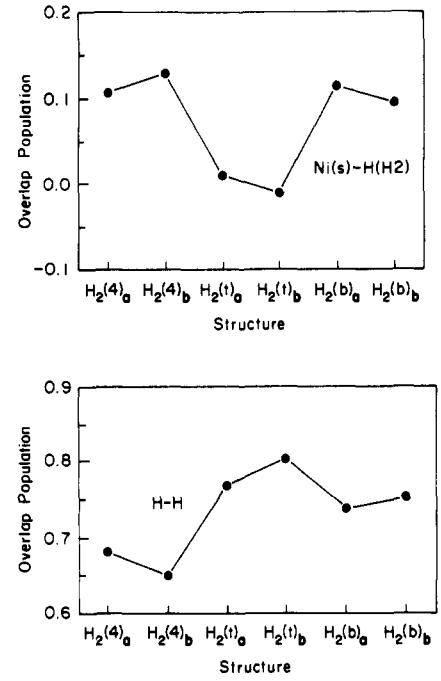

Figure 6. Overlap populations of the Ni(s)–$H(H_2)$ bond (top) and of the H–H bond (bottom) for the six structures.

TABLE V: Electron Energy Loss Data for both Initial and Final Surface States from EELS Experiments and the Overlap Populations Calculated for the Ni(100)/H(4)/CO(t) Structure as Well as the Three Possible Final States

	energy loss, meV	
	initial state	final state
Ni–H(4)	78	67
Ni–CO(t)	50	49
C–O(t)	258	260

	overlap population			
	Ni(100)/ H(4)/CO(t)	$H_2(4)_a$	$H_2(4)_b$	$H_2(t)_a$
Ni–H(4)	0.147	0.145	0.143	0.142
Ni–CO(t)	0.781	0.769	0.758	0.799
C–O(t)	1.080	1.086	1.082	1.075

$H_2(t)$ structures but a negative value for the two higher energy $H_2(b)$ configurations.

Bonding between the surface Ni atoms and the CO(t), CO(4), and H(4) is in fact very similar in all six structures, but there are differences in the hydrogen–hydrogen bonding within an adsorbed H_2 molecule and in the Ni–$H(H_2)$ bonding, where $H(H_2)$ stands for a H atom in H_2. Such differences are presented in Figure 6, where the overlap populations for the H–H and Ni(s)–$H(H_2)$ bonds are plotted. With a negative Ni(s)–$H(H_2)$ overlap population of –0.007, the Ni(s) and $H(H_2)$ interaction in configuration $H_2(t)_b$, one of the $H_2(t)$ structures, is actually slightly repulsive. The structure can therefore be ruled out since the H_2 molecules are known to be chemisorbed.[26] Further evidence can be seen in the H–H curve in the same figure. The overlap population of a H–H bond for the same configuration ($H_2(t)_b$) is higher than that of a gas-phase molecular hydrogen, 0.78. This is not consistent with the HREELS experiments[26] which yield a 487-meV energy loss peak for the chemisorbed H_2, much lower than the gas-phase H_2 frequency of 516 meV.[55,56]

Some of the EELS results for both initial and final state of the Ni(100)/H/CO coadsorbed system are tabulated in Table V, along with the corresponding calculated overlap populations for the Ni(100)/H(4)/CO(t) structure and for the remaining three possible candidates of the final state: $H_2(4)_a$, $H_2(4)_b$, and $H_2(t)_a$.

(55) Avouris, Ph.; Schmeisser, D.; Demuth, J. E. *Phys. Rev. Lett.* **1982**, *48*, 199.
(56) Andersson, S.; Harris, J. *Phys. Rev. Lett.* **1982**, *48*, 545.

CHART VIII

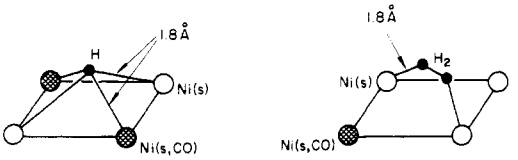

In the final state, the energy loss peak of a terminally bonded C–O is 260 meV, a little higher than that of the initial state, 258 meV. The former 78-meV peak of the Ni–H(4) vibration is now replaced by a smaller one at 67 meV, and a slight decrease in the Ni–CO(t) frequency is also detected: 50 meV before the transformation and 49 meV after. The overlap populations listed give the same trend for the configuration $H_2(4)_a$ and $H_2(4)_b$, although with most change appearing in the Ni–CO(t) bond. Changes in the Ni–CO(t) and C–O(t) bonds for the configuration $H_2(t)_a$ depart from the experimental trend.

Combining all the arguments discussed above, it seems that the 4-fold adsorbed H_2 structures ($H_2(4)_a$ and $H_2(4)_b$) are the most likely choices for the final surface state, although not enough evidence has been found to rule out the possibility of configuration $H_2(t)_a$, a terminally adsorbed H_2 structure.

Differing from other CO/H coadsorption surfaces, the Ni(100)/H/CO system exhibits a unique feature: Σ-desorption around 220 K. This phenomenon was first reported by Yates et al. in 1977.[17] A substantial amount of both adsorbed hydrogen and carbon monoxide desorbs around that temperature—a behavior not observed in the single adsorbate systems. Andersson et al.[26] propose that the Σ-CO desorption is an intrinsic property of the surface, and they attribute the Σ-H_2 desorption to the chemisorbed H_2 species. The hydrogen desorption at higher temperature (~300 K) is similar to the single adsorbate case and is due to the 4-fold adsorbed atomic hydrogens, H(4). The two different H_2 desorption temperatures clearly say something about the relative strength of the nickel–hydrogen bonding in the system:[57] the H(4) atoms are more strongly bonded to the surface than that the $H_2(4)$ molecules are. Let us take structure $H_2(4)_a$, a 4-fold adsorbed H_2 configuration as an example, to see how our analysis agrees with this experimental observation. A local geometry of an absorbed H(4) and a $H_2(4)$ is drawn in Chart VIII. Notice that both H(4) and $H_2(4)$ sit in the 4-fold hollow site, setting up a similar bonding environment for the two. Each $H_2(4)$ is bonded to two surface Ni atoms, Ni(s), with a distance of 1.8 Å, and each H(4) is bonded to two Ni(s) and two Ni(s,CO) atoms with the same Ni–H distance. The distance from the $H_2(4)$ to another two neighboring Ni atoms is longer, and no significant interactions are found. We obtain an overlap population value of 0.107 for the nickel–H(H_2) bond (1.8 Å) and of 0.118 and 0.145 for the Ni(s,CO)–H(4) and Ni(s)–H(4) bonds (1.8 Å), respectively. These results are hardly surprising as an H adsorbate (or ligand in a discrete transition-metal complex) is a much better donor than H_2.

We would like now to explore a little further the surface–adsorbate and adsorbate–adsorbate interactions in one of the most likely final (higher temperature) surface states, that is, the surface structure with 4-fold adsorbed H_2, according to the preceding discussions. This time, let us focus on the structure $H_2(4)_b$. We expect to see a resemblance between $H_2(4)_b$ and $H_2(4)_a$. Shown in Chart IX are two-dimensional views of a proposed initial Ni(100)–p(1×1)H–c(2×2)CO state (**t4** structure) and a c(2√2×√2)R45° structure, $H_2(4)_b$. Notice that the size of the unit cell (the heavy lined frame) is doubled in $H_2(4)_b$. Two H_2 and one CO molecule replace the three H atoms initially found in the 4-fold hollow sites. No significant variations occur in the Ni(s,CO)–CO(t) and Ni–H(4) bonding, nor in the CO(t)–H(4) interactions which have been discussed earlier. This is confirmed in Table VI, where electron densities and crystal orbital overlap populations are compared between the two structures. Indeed, very small changes are detected. What is new is the formation

(57) Private discussions with Bengt Kasemo.

CHART IX

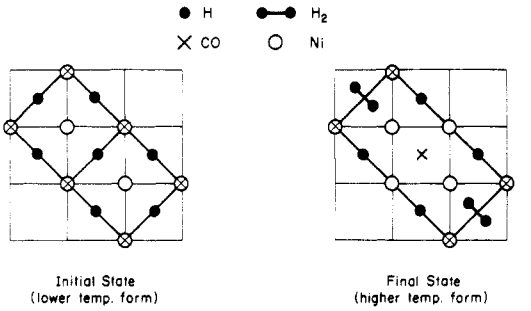

CHART X

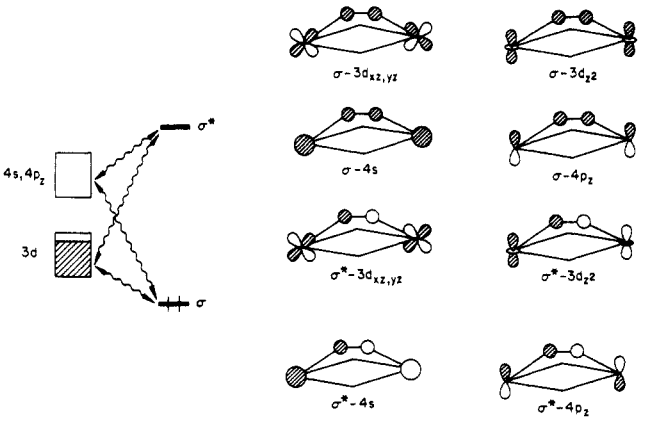

TABLE VI: Electron Densities and Crystal Overlap Populations in the Initial Ni(100)/H(4)/CO(t) State and a c(2√2×√2)R45°CO Structure $H_2(4)_b$

	Ni(100)/H(4)/CO(t)	$H_2(4)_b$
	Electron Density	
CO(t)		
4σ	1.878	1.883
1π	3.999	4.000
5σ	1.567	1.587
2π	0.607	0.617
H(4)		
1s	1.378	1.390
	Overlap Population	
Ni(s,CO)–H(4)	0.124	0.118
Ni(s)–H(4)	0.147	0.145
Ni(s,CO)–C(t)	0.781	0.758
C–O(t)	1.080	1.082
C(t)–H(4)	0.017	0.019

of the Ni(s)–CO(4) and the Ni(s)–$H_2(4)$ bonds. An OP = 0.356 is calculated for the former and an OP = 0.128 for the latter. Both σ and σ* orbitals of a H_2 molecule can interact with Ni(s) 3d as well as its 4s + $4p_z$ states (Chart X). The σ orbital donates electrons to the metal orbitals, and a loss of 0.128 electron results. On the other hand, the back-donation from metal orbitals gives rise to a gain of 0.154 electron to the σ* orbital.

There is another type of adsorbate–adsorbate interaction present in the c(2√2×√2)R45° structure besides the carbon–hydrogen coupling discussed in the previous section, that is, the CO(t)–$H_2(4)$ interaction. Except for the 1π orbitals, 4σ, 5σ, and 2π of a terminally bonded CO are all involved. All of these orbitals are lifted up to some extent, with the 4σ orbital most affected. The density of state projections show that both CO(t) 4σ and $H_2(4)$ σ states spread out over a wide energy region, ~4.5 eV, indicating a fairly strong interactions between the two. However, no real C–H bond is formed. The overlap population of 0.014 suggests a slightly attractive force between the two atoms.

As pointed out earlier, although all three CO(t), CO(b), and CO(4) peaks are observed in the energy loss experiments, it is proposed[26] that the structure is built up primarily of CO molecules at the on-top and 4-fold positions. The argument is that the

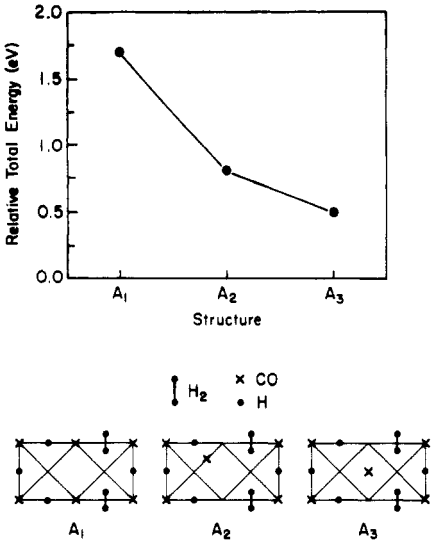

Figure 7. Relative total energies for the three structures A_1, A_2, and A_3. A two-dimensional view of each structure is given in the lower part of the figure.

CHART XI

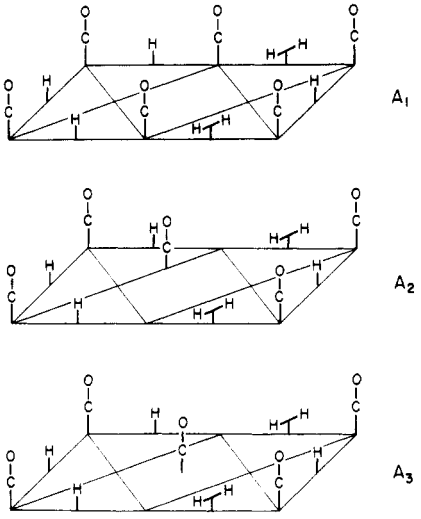

235-meV peak, due to bridge bonded CO, is very weak and can be neglected. Do our analyses agree with this? In Chart XI, we have compared three structures where CO adsorbs in three different sites. In all three structures, half of the CO molecules are fixed in the terminal positions and the other half sit in the on-top, bridging, and 4-fold hollow sites respectively in A_1, A_2, and A_3. The atomic hydrogen and molecular H_2 are also fixed in the 4-fold hollow sites in all three cases. The average total energy plotted in Figure 7 gives the following order: $A_1 > A_2 > A_3$, that is, the CO(t)/CO(4) combination represents the most stable geometry whereas the CO(t)/CO(t) gives the least favorable structural choice. The CO(t)/CO(b) configuration, on the other hand, is only ~0.2 eV higher in its energy than the CO(t)/CO(4) structure according to our calculation. Thus, it cannot be ruled out as a possible final surface state of the coadsorption process.

It has been pointed out that the EELS data show a decrease in the Ni–CO(t) and Ni–H(4) vibrational frequencies and a small increase in the C–O(t) stretching frequency during the structural transformation. In Figure 8, we have plotted the overlap populations of the Ni–H(4), Ni(s,CO)–CO(t), and C–O(t) bonds in the three structures. The corresponding values from the Ni(100)–p(1×1)H–c(2×2)CO structure (**t4**) are also given for each case by a stick. One notices immediately that changes in A_3 [CO(t)/CO(4)] and A_2 [CO(t)/CO(b)] are both consistent with the experiments but not those in the A_1 [CO(t)/CO(t)] structure, where every calculated overlap population varies in the wrong direction (cf. Table V).

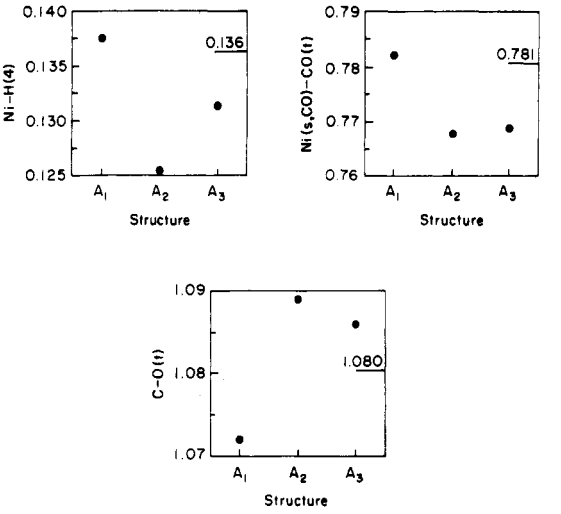

Figure 8. Crystal orbital overlap populations of the Ni–H(4), Ni(s,-CO)–C(t), and C–O(t) bonds in the three structures (A_1, A_2, and A_3). The corresponding values of the **t4** configuration, a Ni(100)–p(1×1)H–c(2×2)CO structure, are also indicated in the plot with a horizontal bar.

TABLE VII: Atomic Parameters Used in the Analyses

orbital	H_{ii}, eV	ζ_1	ζ_2	c_1[a]	c_2[a]
Ni(4s)	−7.8	2.1			
Ni(4p)	−3.7	2.1			
Ni(3d)	−9.9	5.75	2.00	0.5683	0.6292
C(2s)	−18.2	1.63			
C(2p)	−9.5	1.63			
O(2s)	−29.6	2.27			
O(2p)	−13.6	2.27			
H(1s)	−13.6	1.30			

[a] Coefficients of the double-zeta function of the d orbitals.

Both energy and overlap population analyses provided above seem to agree that the CO(t)/CO(t) geometry, A_1, is most unlikely to be a stable final state. The CO(t)/CO(b) structure, A_2, on the other hand, may appear in the final surface state.

Conclusions

Our calculations for the coadsorption of carbon monoxide and hydrogen on the Ni(100) surface give the lowest energy for the **t4** geometry, a Ni(100)–p(1×1)H–c(2×2)CO surface structure which has been suggested by various experimental techniques to be the low-temperature form in the coadsorption process. The surface–adsorbate interactions resemble what have been described in the single adsorbed systems, that is, the metal–CO bonding comes mainly from the $3d_{z^2}$–5σ (σ-type) and $3d_{xz,yz}$–2π (π-type) interactions and the metal–H bonding comes from the $3d_{xy}$–1s interaction. The adsorbate–adsorbate interactions, mostly attributed to the CO(t) 2π and the H(4) 1s states, do not lead to any C–H or O–H bonds but do result in a destabilization of the CO(t) 2π orbitals. The consequence of this is weakening of the π-type bonding between the surface metal and the adsorbed CO and a slight strengthening of the C–O bond.

The structural transformation occurring at higher temperature (~150 K) leads to a new surface state, Ni(100)–H,H_2–c(2√2×√2)R45°CO. Energetically, we find that the 4-fold adsorbed H and H_2 [or H(4) and H_2(4)] surface configurations $H_2(4)_a$ and $H_2(4)_b$ represent the most favorable structural choices. We cannot, however, rule out one of the H_2(t) geometries, i.e., the configuration $H_2(t)_a$. A new type of adsorbate–adsorbate coupling is observed between the on-top adsorbed CO and the 4-fold adsorbed H_2 in structure $H_2(4)_b$ (as well as in $H_2(4)_a$), but again, no chemical bonds are formed. Bridging CO has been observed in the EELS experiments, and our calculations suggest the possibility of the CO(t)/CO(b) combination in the final state, although the CO(t)/CO(4) structure represents the best choice computed from both energy and crystal orbital overlap population analyses.

Acknowledgment. J.L. and R.H. are grateful to the Office of Naval Research for its generous support of this work. B.S. expresses her thanks to Thanks to Scandinavia (especially Mr. Richard Netter), who has made her stay at Cornell possible, and D.M.P. to NATO for its support through Grant 200.81. We thank Jane Jorgensen and Elisabeth Field for their expert drawings.

Appendix

The extended Hückel tight-binding approach is employed in this study. The Ni-C, Ni-H, and C-O bond distances are kept the same in all geometries, and these are 1.8, 1.8, and 1.15 Å, respectively. The H-H distance in an adsorbed H_2 molecule is taken to be 0.74 Å. Other atomic parameters are summarized in Table VII. For the average property calculations two 16 k-point sets are selected according to the geometrical method by Ramirez and Böhm.[58]

Registry No. CO, 630-08-0; H_2, 1333-74-0; Ni, 7440-02-0.

(58) Ramirez, R.; Böhm, M. C. *Int. J. Quantum Chem.* **1986**, *30*, 391.

Interaction of Mn with the Ru(001) Surface and Chemisorption of CO on the Mn/Ru(001) Interface

Jan Hrbek

Department of Chemistry, Brookhaven National Laboratory, Upton, New York 11973
(Received: May 16, 1989; In Final Form: September 6, 1989)

The interaction of vapor-deposited Mn with the Ru(001) surface and its effect on CO chemisorption were studied under ultrahigh vacuum by Auger electron spectroscopy (AES), thermal desorption spectroscopy (TDS), isotopic exchange, and low-energy electron diffraction (LEED). At room temperature, Mn grows layer by layer. The first three layers are pseudomorphic with respect to the Ru substrate. At higher coverages, manganese layers adopt a commensurate structure with a $(\sqrt{3}\times\sqrt{3})R30°$ LEED pattern. At coverages of more than 10 layers, the growing layer of manganese becomes disordered. Disordered and $\sqrt{3}$ structures are thermally unstable, and annealing to 700 K leads to their transformation to a (1×1) pseudomorphic structure, together with a large decrease in the Mn/Ru AES ratio. A complete analysis of Mn thermal desorption data shows that there is a decrease of the heat of adsorption with increasing coverage within the first monolayer (69 to 55 kcal/mol) and zero-order desorption for higher coverages with desorption energy 54 kcal/mol. A new, higher temperature CO desorption state at 650–800 K appears at submonolayer coverages. The C–O bond of CO chemisorbed on Mn/Ru is severely weakened and probably dissociated as evidenced by a high CO desorption temperature and random isotope mixing of coadsorbed isotopes of carbon monoxide.

Introduction

In recent years there have been numerous experiments on bimetallic and alloy surfaces because of the fundamental importance of these systems in catalysis and in corrosion processes. Bimetallic catalytic systems are superior to their single-component counterparts as practical catalysts.[1] The goal of recent surface science studies is to understand the origin of their behavior on a microscopic scale. A typical example is the bimetallic Cu/Ru system,[2,3] for which it was shown that a single layer of Cu on a Ru substrate no longer retains the chemisorptive and electronic properties of Cu bulk metal.

The Ru catalyst is known for its high activity in the hydrogenation reactions of carbon monoxide and nitrogen.[4] For that reason its electronic and chemisorptive properties have been studied by several groups in the past decade.[5-9] Besides its interesting surface chemistry, the large surface free energy (3.4 J/m^2)[10] of ruthenium renders it a valuable substrate in the model studies of bimetallic systems. Consequently, there have been a number of recent studies of the interaction of Ru with various metals, namely, Cu,[2,3] Ag,[11] Au,[12] Pd,[10] Ni,[13] Fe,[14-17] Ti,[17] Al,[18] and Mn.[19,20]

The chemisorption of CO on clean Ru(001) has been characterized in great detail with many surface-sensitive probes.[5-8] Chemisorption is molecular with a coverage-dependent desorption energy; there is a saturation coverage of 0.58 CO per Ru surface atom at room temperature, and its desorption has two characteristic peaks at 400 and 460 K, which reflect lateral CO–CO repulsion at coverages above $\theta_{CO} > 1/3$.[8] In contrast to the wealth of data on Ru, there is little information on CO chemisorption on well-characterized Mn surfaces.[21] Judging from the stretching frequency of CO adsorbed on a Mn film, the adsorption seems to be molecular.[22]

Experimental Section

The experiments were performed in an ultrahigh-vacuum system with a base pressure better than 1×10^{-10} Torr that was equipped with a single-pass cylindrical mirror analyzer for AES, LEED

(1) Sinfelt, J. H. *Bimetallic Catalysts. Discoveries, Concepts and Applications*; Wiley: New York, 1983.
(2) Christmann, K.; Ertl, J.; Shimizu, H. *J. Catal.* **1980**, *61*, 397.
(3) Houston, J. E.; Peden, C. H. F.; Blair, D. S.; Goodman, D. W. *Surf. Sci.* **1986**, *167*, 427.
(4) Bond, G. C. *Heterogeneous Catalysis. Principles and Applications*, 2nd ed.; Clarendon Press: Oxford, 1987.
(5) Madey, T. E.; Menzel, D. *Jpn. J. Appl. Phys.* **1974**, Suppl. 2, Part 2, 229.
(6) Williams, E. D.; Weinberg, W. H. *Surf. Sci.* **1979**, *82*, 93.
(7) Pfnur, H.; Menzel, D.; Hoffmann, F. M.; Ortega, A.; Bradshaw, A. M. *Surf. Sci.* **1980**, *93*, 431.
(8) Pfnur, H.; Feulner, P.; Menzel, D. *J. Chem. Phys.* **1983**, *79*, 4613.
(9) Anton, A. B.; Avery, N. R.; Madey, T. E.; Weinberg, W. H. *J. Chem. Phys.* **1986**, *85*, 507.
(10) Park, C. *Surf. Sci.* **1988**, *203*, 395.
(11) Niemantsverdriet, J. W.; Dolle, P.; Markert, K.; Wandelt, K. *J. Vac. Sci. Technol.* **1987**, *A5*, 875.
(12) Harendt, C.; Christmann, K.; Hirchwald, W.; Vickermann, J. C. *Surf. Sci.* **1986**, *165*, 413.
(13) Berlowitz, P. J.; Goodman, D. W. *Surf. Sci.* **1987**, *187*, 463.
(14) Egawa, C.; Aruga, T.; Iwasawa, Y. *Surf. Sci.* **1987**, *188*, 563.
(15) Egawa, C.; Iwasawa, Y. *Surf. Sci.* **1988**, *195*, 43.
(16) Harrison, K.; Prince, R. H.; Lambert, R. M. *Surf. Sci.* **1988**, *201*, 393.
(17) Badyal, J. P. S.; Gellman, A. J.; Lambert, R. M. *J. Catal.* **1988**, *111*, 383.
(18) Campbell, C. T.; Goodman, W. D. *J. Phys. Chem.* **1988**, *92*, 2569.
(19) Hrbek, J. *J. Vac. Sci. Technol.* **1987**, *A5*, 865.
(20) Hrbek, J.; Sham, T. K.; Shek, M.-L. *Surf. Sci.* **1987**, *191*, L772.
(21) Baker, F. S.; Bradshaw, A. M.; Pritchard, J.; Sykes, K. W. *Surf. Sci.* **1968**, *12*, 426.
(22) Bickley, R. I.; Roberts, M. W.; Storey, W. C. *J. Chem. Soc. A* **1971**, 2774.

0022-3654/90/2094-1564$02.50/0